Desalination and Water Treatment
www.deswater.com

doi:10.5004/dwt.2019.23258

139 (2019) 327–341
January

Statistical design of experiment as a tool for optimization of methylene blue sorption on CS/MCM-41/nano-γ alumina as a novel and environmentally friendly adsorbent: isotherm and kinetic studies

Abbas Teimouri[a,*], Nahid Ghased[a], Shima Ghanavati Nasab[b], Saeed Habibollahi[a]

[a]*Chemistry Department, Payame Noor University, 19395-3697, Iran, Tel. +98 31 33521804, Fax +98 31 33521802, email: a_teimouri@pnu.ac.ir, a_teimoory@yahoo.com (A. Teimouri), nahid.ghased@gmail.com (N. Ghased), saeedehabibollahi@yahoo.com (S. Habibollahi)*

[b]*Department of Chemistry, Faculty of Sciences, University of Shahrekord, P. O. Box 115, Shahrekord, Iran, email: shima.gh363@gmail.com*

Received 3 September 2017; Accepted 10 October 2018

ABSTRACT

Chitosan/Mesoporous silica/Nano-γ alumina was synthesized and characterized by FTIR, XRD, FESEM, TGA and BET; also, it was applied as an efficient and eco-friendly adsorbent to investigate the adsorption properties of Methylene blue (MB) from the aqueous solution by following the optimization of influential parameters such as pH, contact time, adsorbent mass, and the initial concentration of MB by the central composite design (CCD) under a response surface methodology (RSM). Maximum removal efficiency at the optimum conditions (pH: 7.5, contact time: 45 min, adsorbent dosage: 0.088 mg, and the initial dye concentration: 15 mg/L) was achieved to be 90.23%. Analysis of variance and calculation of the correlation coefficient related to the predicted and experimental values of the removal percentage of MB proved the precision of the equation acquired by CCD. Subsequently, it was found that the adsorption isotherm was well fitted, and it was in a good agreement with the Langmuir isotherm model; the maximum adsorption efficiency (q_{max}) was found to be 80 mg/g. The study of the relation between time and the adsorption rate indicated that the adsorption of MB onto CS/MCM-41/Nano-alumina obeyed the pseudo-second-order. Besides, thermodynamic parameters calculated in this research, including ΔG°, ΔH°, and ΔS° revealed that the adsorption of MB on the adsorbent was spontaneous and endothermic. According to the results obtained in this research, CS/MCM-41/Nano-alumina could be regarded as an effective adsorbent for MB elimination from the aqueous solution.

Keywords: Chitosan; MCM-41; Nano-γ alumina; Removal; Methylene blue; Central composite design

1. Introduction

The aromatic compounds with major groups, such as azo, antracoeinin, triarilen ethane and phetalosisanin are called dye. Different industries such as textile, printing, paper, plastic, and food are introducing more than 7×10^5 (tons per year) chromophore. Among these, the textile industry releases the highest amount of the dye effluent into the environment [1]. Nowadays, the presence of hazardous dyes in the effluent of industries has been the most important environmental danger [2]. The existence of dyes in water can be noxious for both human and environment owing to serious adverse health problems [3]. Hence, it is critical to remove toxic dyes to make a friendly environment. Methylene blue (Fig. 1) belongs to cationic dyes applied in coloring paper, cottons, and wools. The solution of this odorless powder in water is blue. Although MB is not very poisonous, the extermination and removal of that from the aqueous solution is essential. This is because it has some harmful effects including diarrhea, cyanosis, tissue necrosis, vomiting, jaundice, quadriplegia, shock and raised heart rate in the human being [2,4].

*Corresponding author.

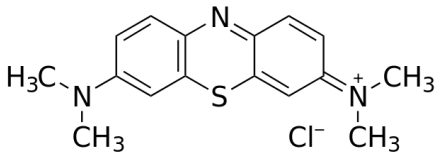

Fig. 1. Chemical structure of MB.

Several methods have been recently used for the removal of toxic dyes from the effluents of industries; these include flocculation, photo catalytic degradation, adsorption, membrane filtration, reverse osmosis, etc. [5]. Among these, adsorption is one of the strategies vastly utilized because it has some advantages; for example, ease of operation, low cost, and good removal efficiency [6]. Therefore, greenness, nontoxicity, low cost, and high adsorption efficiency are demanded for any adsorbents in order to eliminate any pollutants [7]. So, nanoparticles-based adsorbents can be desirable candidates for the removal of diverse poisonous materials, because they have a large surface area with a large number of reactive atoms and a high number of unoccupied reactive surface sites which can improve the adsorption capacity [8]. Therefore, they can be used as efficient adsorbents for the removal of various pollutants [9]. It is necessary to introduce a novel and frugal adsorbent for the improvement of contaminants. Recently, the sorption based on natural polymers such as chitosan has been of interest to researchers. Chitosan is a plentiful biopolymer produced from the alkaline N-deacetylation of chitin, which is the second copious polymer in nature and is obtained from crustacean like prawns, crabs, fungi and insects. Chitosan has some unique merits including biodegradability, biocompatibility and non-toxicity. Hence, it has been extensively used in water purification. The adsorption capacity of chitosan for the removal of contaminants is 1000–1100 g/kg. This high adsorption efficiency is related to the presence of hydroxyl and amino groups on the surface, binding with different pollutants. However, chitosan has some serious downsides in terms of mechanical strength and solubility in acidic media that can restrict its adsorption performance. Chemically cross linking the reaction of chitosan by appropriate cross linking agents can improve its chemical and mechanical problem. Nevertheless, this action decreases the sorption capacity of chitosan owing to the reaction of the cross linking agent with the a mine group (main adsorption sites) of chitosan. Addition of particular functional groups by grafting is essential after cross linking to solve this problem and can enhance the mentioned dye sorption characteristics [10–14]. For this purpose, in this study, chitosan combined with MCM-41 and nano-γ alumina was prepared and used as a novel adsorbent for the elimination of MB. In fact, Mesoporous silica (MCM-41), belonging to a mesoporous material group, has high surface area and reactive sites due to the presence of Si-O and Si-OH groups as the main sites for the removal of MB; it possesses a regular hexagonal array of cylindrical pores, so it can be greatly used in the selective adsorption [15]; it has been introduced to combine with chitosan for loading nano-γ alumina. It is expected that removal efficiency by CS/MCM-41/nano-γ alumina would be intensified, as compared to neat chitosan, due to the synergistic effects of nanocomposite that would arise from large surface area and the reactive sites of nanocomposite, as well as the high porous structure of the adsorbent.

Conventional and classical methods of optimization (one at a time) are not able to present useful information regarding the interaction between parameters, leading to great labor and wasting much time due to the high number of experiments required. The central composite design (CCD) under the response surface methodology (RSM) can be effectively used for managing both variables included and responses, without suffering from the above-mentioned disadvantages. This technique can evaluate the relationships among the experimental variables and responses, giving the main interaction influences. It is feasible to make a mathematical equation showing the association between parameters and responses by applying a small amount of reagents [4,16].

In continuation of our previous works in removal [17–19], in the present study, CS/MCM-41/nano-γ alumina was synthesized and characterized by FTIR, FESEM, XRD and BET analysis. The influence of four parameters such as pH, the initial dye concentration, contact time, and the adsorbent dosage was studied and optimized by the central composite design (CCD) to achieve the optimal conditions for the maximum removal performance of MB. In addition, the adsorption process was estimated by the adsorption dynamic model, the adsorption isotherm model, and adsorption thermodynamics. Finally, a comparison of the influence of other adsorbents on the removal of MB has been made.

2. Experimental

2.1. Materials and apparatus

Medium molecular weight chitosan with the deacetylation degree of 85–95%, gamma alumina powder (<100 nm), and MCM-41 were prepared from Sigma-Aldrich chemicals. All other chemicals including boric acid, citric acid, phosphate sodium twelve hydrate, methylene blue, ethanol and methanol were of the analytical grade and purchased from Merck. Double distilled water was utilized for the preparation of all solutions.

SEM images were obtained by using a field emission SEM (VEGA//TESCAN-LUM). Fourier transform infrared spectroscopy (FTIR) of the adsorbent was recorded by an FTIR spectrophotometer (JASCO FTIR-680 PLUS). X-ray diffraction (XRD) patterns of the samples were acquired using a Philip X-Pert X-ray diffractometer (ASENWARE AW-XDM300) with Cu *K*α radiation (40 KV) for 2θ values over 0–80°.

The BET specific surface areas and BJH pore size distribution of the nanocomposite were rated by applying a series BEL: PHS1020. The thermal behavior of ZN/CS/nHAp composite scaffolds was carried out using a DuPont TGA 951. The temperature was raised from room temperature to 800°C in air and at a heating rate of 10°C/min. The pH measurements were done using a pH meter, the model 826 (Metrohm, Switzerland, Swiss), and the MB concentrations were assessed by a UV-Visible spectrometer, the model UV-2550, at the wavelength of 674 nm. An ultrasonic bath with heating system (Tenco-GAZ SPA Ultra Sonic Sys-

tem), at the frequency of 40 kHz and the power of 130 W, was employed for the ultrasound-assisted adsorption procedure.

2.2. Preparation of adsorbent

2.2.1. Synthesis of MCM-41

MCM-41 was prepared as follows: Cetyltrimethylammonium bromide ($C_{19}H_{42}BrN$, CTAB) was used as the template. The template was dissolved in 120 g deionized water to obtain a clear solution and 10 mL of aqueous ammonia was added to the solution. While stirring, 10 mL tetraethyl orthosilicate (TEOS) was added to the surfactant solution over a period of 24 h. The resulted white gel was spilled into a Teflon recipient hermetically closed and heated at 70°C for 48 h until the hydrolysis and condensation of silica were completed. The obtained material was filtered, washed with H_2O and ethanol, and dried. The product in this step was named MCM-41. Afterwards, the surfactant was removed from the mesoporous material by heating the sample in an oven at 550°C for 6 h until the surfactant was completely deleted [20,21].

2.2.2. Preparation of CS/MCM-41/Nano-γ alumina

CS/MCM-41/Nano-γ alumina was prepared via the co-precipitation method. Three molar ratios of the nanocomposite, including CS/MCM-41(70%)/nano-γ alumina (30%), CS/MCM-41 (50%)/nano-γ alumina (50%) and CS/MCM-41 (30%)/nano-γ alumina (70%), were prepared. For example, to synthesize the CS/MCM-41 (70%)/nano-γ alumina (30%) nanocomposite, 0.3 g of nano-γ alumina was dissolved in 0.7 g of MCM-41 while it was stirred for 1 h. Later, 1 g of CS solution, as prepared by dissolving in the acetic acid using ultrasonic bath, was poured into the mixture of MCM-41/nano-alumina and 25% glutaraldehyde was added by keeping stirring for 1 h to obtain the CS/MCM-41(70%)/nano-γ alumina(30%) nanocomposite. Finally, the nanocomposite beads were dried and ground [22–24].

2.3. Determination of point of zero charge

The isoelectric point (pH_{IEP}) i.e. point of zero charge (pH_{PZC}) indicates the ability of the surface to adsorb the adsorbate [25]. The pH of a series of ten Erlenmeyer flasks containg 15 mL NaCl 0.1 mol L^{-1} as electrolyte solutions was adjusted in the range of 4–9 using NaOH or HCl (0.1 mol L^{-1}) and it was considered as initial pH of the solution. To reach the equilibrium state the solutions were let for 24 h. Consequently, the final pH of the solutions was determined after the specific time [26]. The pH_{PZC} was obtained 6.50.

At pH lower than 6.50, the cationic dyes are in competition with the H^+ ions present in high concentration in the solution. These hydronium ions are thus more adsorbed than the cationic dyes because of their high mobility. On the other hand, in the pH_{PZC} the cationic dyes are eliminated by the OH^- ions. Moreover, when the pH increases (over 6.50), there is a decrease in the H^+ cations, which shows the increase in the adsorption amount of methylene blue.

2.4. Adsorption of MB studies

The dye concentration was obtained from the calibration curve (the plot of absorbance vs. MB concentration) achieved at the maximum wavelength over the working concentration range. Removal efficiency of MB was estimated by determining the concentration of the dye before and after adsorption by the adsorbent. To obtain the MB dye removal, the following equation could be applied:

$$\text{MB removal (\%)} = ((C_0 - C_1)/C_0) \times 100 \quad (1)$$

where C_0 and C_1 (mg/L) are the concentrations of MB before and after the adsorption, respectively.

To evaluate the adsorbed amount of MB, q_e *(mg/g)*, the following equation can be utilized:

$$q_e = (C_0 - C_e)\, V/W \quad (2)$$

where C_0 and C_e (mg/L) are the initial and equilibrium concentrations of MB in the solution, respectively. V (L) is the volume of the solution and W (g) is the mass of the adsorbent.

2.5. Comparison of removal of methylene blue by three molar ratios of CS/MCM-41/nano-γ alumina nanocomposites and determination of optimized ratio

Before optimizing the numerical factors like pH, MB concentration, adsorbent dosage and contact time, it was needed to determine the best molar ratio of the CS/MCM-41/nano-γ alumina nanocomposite for the removal of MB. As can be seen in Fig. 2, the best molar ratio was CS/MCM-41(70%)/nano-γ alumina(30%). So, optimizing the conditions of removal by the CCD method could be done by this ratio of the adsorbent.

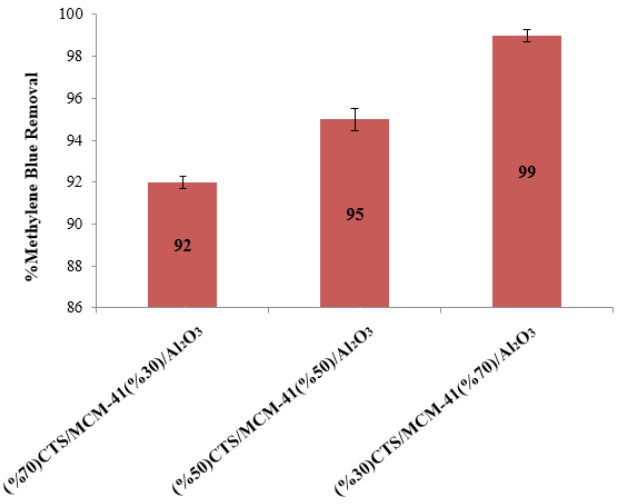

Fig. 2. The influence of three molar ratios of the CS/MCM-41/nano-γ alumina nanocomposite on the adsorption performance for removal of MB. Concentration: 10 mg/L; adsorbent dosage: 0.1 g; pH: 7; contact time: 30 min; temperature: 25°C.

2.6. Response surface methodology

The main objective of using the design of experiment was to decrease the number of experiments and to consider the important parameters in the research, instead of several experiments which would consume time and could, in fact, be boring. Central composite design (CCD) in RSM is the most popular class of design used for fitting a second order model [27]. In the present work, four important variables were regarded in the experiments with five levels. The ranges and levels of each independent parameter with actual and coded values are shown in Table 1. The independent parameters were coded to two levels: low (–1) and high (+1), since the axial points were coded as –2 and +2. A five-level-four-factor central composite design was applied to suit a second order response surface model that needed 30 experiments, which included 16 factorial, 8 axial points and 6 replicates at the center points, to appraise the experimental error and the reproducibility of the data. 30 experiments were done in the random order and the removal efficiency was obtained. The mathematical relationship between the four independent variables was estimated by the second-order polynomial model [28]:

$$Y = \beta_0 + \sum_{i=1}^{n}\beta_i x_i + \sum_{i=1}^{n}\sum_{j=1}^{n}\beta_{ij} x_i x_j + \sum_{i=1}^{n}\beta_{ii} x_i^2 + \varepsilon \quad (3)$$

where Y is the predicted response (R%), and x_i and x_j are the coded values for the experimental factors (pH, the initial concentration of the dye, contact time and adsorbent mass). β_0 is the model constant, β_i is the linear coefficient, β_{ii} is the quadratic coefficient, β_{ij} is the cross-product coefficient, ε is the residual term, and n is the number of variables. The response surface methodology (RSM) permits the estimation of the relative factors significance and application of multivariate equation to acquire an optimum response [29]. The experiment was done for six times. The complete CCD design matrix in terms of the real independent factor and the related outcomes are presented in Table 2. The modeling was carried out by the adjustment of the first or second-order polynomial equation to the experimental responses. Analysis of variance (ANOVA), regression analysis, and plotting of 3D plot were utilized to establish the optimum conditions for the dye removal. The accuracy and general ability of the polynomial model were rated by the coefficient of determination (R^2) (Table 3).

3. Results and discussion

3.1. Characterization of the adsorbent

3.1.1. FTIR analysis

FTIR spectrometry was applied to obtain information regarding the chemical characterization of the synthesized adsorbent. FTIR spectra of neat CS, MCM-41 and Nano alumina, and FTIR spectra of the two components of each element of the nanocomposite, as well as the mentioned nanocomposite with the various molar ratios of Nano-γ alumina, are presented in Figs. 3A, B, and C, respectively. FTIR

Table 2
Central composite design and the observed and predicted values for removal efficiency (%) of MB by CS/MCM-41/Nano-γ alumina.

Run	Block	Factors				Removal efficiency (%)
		X_1	X_2	X_3	X_4	
1	First day	7.50	10.00	0.0065	40.00	83.90
2	First day	4.50	20.00	0.0065	40.00	30.00
3	First day	6.00	15.00	0.0077	45.00	81.00
4	First day	4.50	10.00	0.0065	50.00	42.00
5	First day	6.00	15.00	0.0077	45.00	81.90
6	First day	4.50	10.00	0.0090	40.00	61.00
7	First day	7.50	10.00	0.0090	50.00	87.80
8	First day	7.50	20.00	0.0065	50.00	85.00
9	First day	7.50	20.00	0.0090	40.00	86.00
10	First day	4.50	20.00	0.0090	50.00	63.00
11	Second day	7.50	20.00	0.0090	50.00	88.00
12	Second day	6.00	15.00	0.0077	45.00	80.00
13	Second day	7.50	20.00	0.0065	40.00	82.00
14	Second day	4.50	10.00	0.0065	40.00	39.00
15	Second day	4.50	20.00	0.0090	40.00	56.00
16	Second day	4.50	10.00	0.0090	50.00	71.90
17	Second day	4.50	20.00	0.0065	50.00	35.00
18	Second day	7.50	10.00	0.0065	50.00	87.00
19	Second day	7.50	10.00	0.0090	40.00	88.00
20	Second day	6.00	15.00	0.0077	45.00	83.00
21	Third day	6.00	25.00	0.0077	45.00	78.00
22	Third day	6.00	15.00	0.0077	45.00	82.00
23	Third day	3.00	15.00	0.0077	45.00	17.00
24	Third day	6.00	15.00	0.0053	45.00	65.00
25	Third day	6.00	15.00	0.0077	55.00	77.00
26	Third day	9.00	15.00	0.0077	45.00	89.00
27	Third day	6.00	15.00	0.0077	45.00	77.80
28	Third day	6.00	5.00	0.0077	45.00	84.00
29	Third day	6.00	15.00	0.0077	35.00	70.00
30	Third day	6.00	15.00	0.0102	45.00	82.00

Table 1
Experimental factors and levels in the central composite design

Factors	Symbol	Levels				
		−α	Low (–1)	Central (0)	High (+1)	+α
pH	X_1	3.0	4.5	6.0	7.5	9.0
MB concentration, mg/L	X_2	5.0	10.0	15.0	20.0	25.0
Adsorbent dosage, g	X_3	0.0053	0.0065	0.0077	0.0090	0.0102
Contact time, min	X_4	35.0	40	45.0	50.0	55.0

Table 3
ANOVA of the second-order polynomial equation for removal efficiency (%) of MB by CS/MCM-41/Nano-γ alumina.

Source	SS[a]	Df[b]	MS[c]	F-value	p-Value	Remark
Block	20.62	2	10.31			
Model	11197.54	14	799.82	102.96	< 0.0001	Highly significant
X_1	7840.94	1	7840.94	1009.32	< 0.0001	Highly significant
X_2	94.41	1	94.41	12.15	0.0040	Significant
X_3	960.14	1	960.14	123.59	< 0.0001	Highly significant
X_4	95.20	1	95.20	12.25	0.0039	Significant
X_1X_2	36.60	1	36.60	4.71	0.0491	Significant
X_1X_3	552.25	1	552.25	71.09	< 0.0001	Highly significant
X_1X_4	20.25	1	20.25	2.61	0.1304	Significant
X_2X_3	1.10	1	1.10	0.14	0.7125	Not significant
X_2X_4	2.500E-003	1	2.500E-003	3.218E-004	0.9860	Not significant
X_3X_4	1.96	1	1.96	0.25	0.6239	Not significant
X_1^2	1496.92	1	1496.92	192.69	< 0.0001	Highly significant
X_2^2	4.12	1	4.12	0.53	0.4795	Not significant
X_3^2	140.40	1	140.40	18.07	0.0009	Significant
X_4^2	140.40	1	140.40	18.07	0.0009	Significant
Residual	100.99	13	7.77			
Lack of Fit	87.27	10	8.73	1.91	0.3246	Not significant
Pure Error	13.73	3	4.58			
Cor Total	11319.15	29				

$R^2 = 0.9911$, Adj $R^2 = 0.9814$, Pred $R^2 = 0.9429$.
[a]Sum of square, [b]Degree of freedom, [c]Mean square.

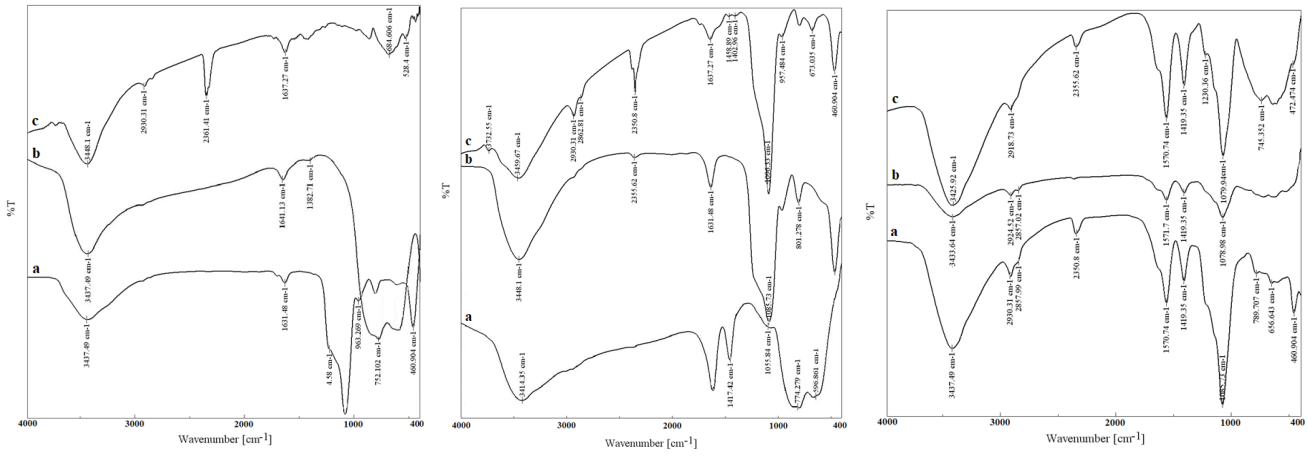

(a) (b) (c)

Fig. 3. FTIR spectra of A: a) MCM-41, b) nano-alumina and c) Chitosan; B: a) CS/nano-alumina, b) MCM-41/nano-alumina and c) CS/MCM-41; C: a) CS/MCM-41 (70%)/nano-alumina (30%), b) CS/MCM-41 (50%)/nano-alumina (50%) and c) CS/MCM-41 (30%)/nano-alumina (70%).

spectra of the neat CS, as presented in Fig. 2A:c, indicated some characteristic peaks including the bands at 3448 cm^{-1} which were related to the stretching vibration modes of OH and NH, the band at 1637 cm^{-1} that could be ascribed to the NH bond of the acetyl group (bending vibrations), and the band at 2930 that could be attributed to the stretching vibration of aliphatic CH bonds [30]. In the spectrum of MCM-41 shown in Fig. 3A:a, there were two important peaks related to the stretching vibration of OH in silanol (Si-OH) groups that appeared at 3437 and 1631 cm^{-1}; also, symmetric and asymmetric stretching bonds of Si-O-Si groups, as presented at 963 and 750 cm^{-1}, respectively, could be seen [31]. The prominent area for nano alumina appeared in a wave number range from 500-1000 cm^{-1} and could be ascribed

to the vibration of aluminum oxide. The bending mode of O-Al-O and the stretching vibration of Al-O were recorded at 665 and 752 cm^{-1}. The band at 3437 cm^{-1} corresponded to the stretching vibration of the OH group, as shown in Fig. 3A:b [9]. The spectrum of the two components, as given in Fig. 3B, was slightly little different from that of pure materials, but the characteristic peaks of the neat components appeared in the spectrum. However, the location of characteristic bands changed slightly and the peak height was reduced owing to the modification of CS with MCM-41 and nanoalumina. In the spectra of CS/Nanoalumina, as shown in Fig. 3B:a, the bands related to CS and nanoalumina were shown at 1417, 3414 and 774. In the spectra of MCM-41/Nano alumina, as given in Fig. 2B: b, the peaks at 3448, 1631, 1085, 801 and 460 cm^{-1} were attributed to MCM-41 and nanoalumina. The peaks at 2930 and 1637 could be ascribed to CH stretching vibration and NH_2 bending vibration in CS; as well, the bands at 963 and 752 cm^{-1} were related to the symmetric and asymmetric stretching vibrations of Si-O-Si in MCM-41, and they could be recorded in the spectra of MCM/CS, as presented in Fig. 3B: c. As can be seen in Fig. 3C, the intensity of the peaks of the nanocomposite varied with a change in the molar ratio of nanoalumina. It was obvious that the intensity of the characteristic bands of nanoalumina was enhanced with the increase in the molar ratio of that and vice versa. It was also found that the major bands of pure CS, MCM-41 and nanoalumina could be observed in the spectra of the nanocomposite.

3.1.2. XRD analysis

X-ray pattern of the synthesized nanocomposite with different molar ratios of nano-alumina to MCM-41 is given in Fig. 4B: a, b, and c. As it is clear in Fig. 3B:c, in the X-ray spectrum of CS/ MCM-41/Nano-alumina with the content of 30 wt% MCM-41 and 70% nanoalumina, some main peaks at 2θ = 41.5237, 26.0825, 21.5960, 19.8044 and 10.1396 were assigned to CS; peaks at 2θ = 67.10, 46.40 and 37.50 were related to nano-alumina. X-ray peaks of MCM-41 at 2θ = 2.2 and 6.2 were observed, confirming the existence of CS, nano-alumina and MCM-41 in the structure of the synthesized nanocomposite. It could also be concluded that the height and intensity of the characteristic peaks of alumina were elevated by the enhancement of the molar ratio of nano-alumina to CS/MCM-41. The XRD patterns of MCM-41/nano-alumina, CS/nano-alumina, CS/MCM-41, and MCM-41 in the optimum nanocomposite, as shown in Fig. 4A and C, were obtained as well.

3.1.3. FESEM analysis

FESEM helped us to obtain information regarding the morphology and particle size of the nanocomposite and to confirm the modification of the surface of CS. The FESEM images of CS/MCM-41/nano-alumina before adsorption with diverse molar ratios of nano-alumina to MCM-41 and FESEM image of the nanocomposite after the adsorption of MB were prepared, as given in Figs. 5a, b, c; also, dispersion of MCM-41 and nano-alumina into CS and the presence of particles less than 100 nm could be seen in Figs. 5a, b, and c. In fact, CS served as a bed/support for MCM-41 and

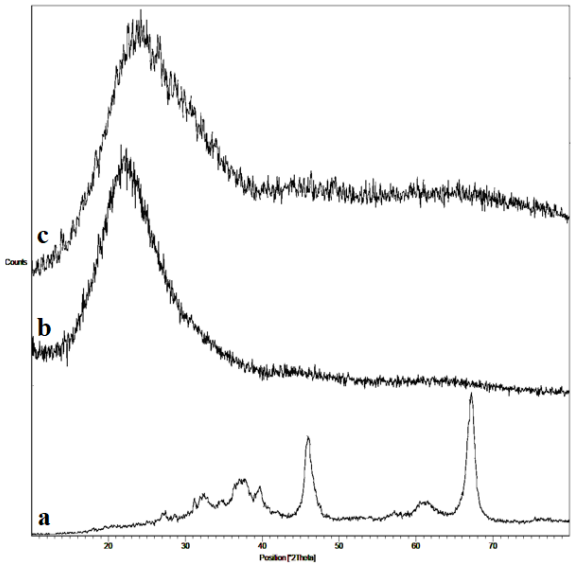

(a)

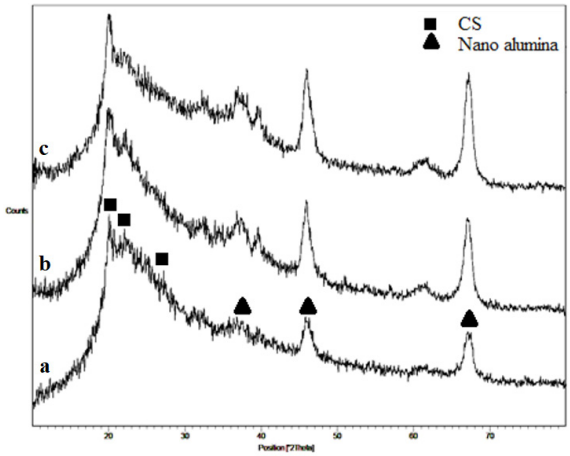

(b)

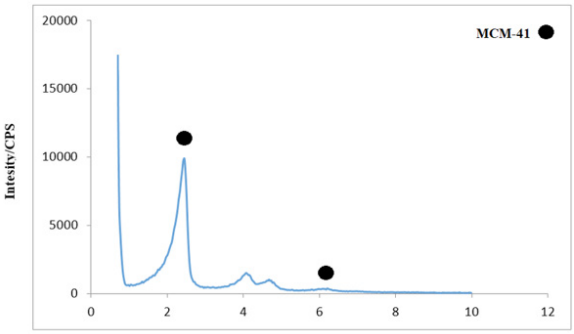

(c)

Fig. 4. XRD patterns of A: a) MCM-41/nano-alumina, b) CS/nano-alumina, and c) CS/MCM-41;B:a) CS/MCM-41 (70%)/nano-alumina (30%), b: CS/MCM-41 (50%)/nano-alumina (50%), c: CS/MCM-41 (30%)/nano-alumina (70%); C: pure MCM-41 in the optimum nanocomposite.

nano-alumina; due to its broad surface, and dispersion of MCM-41 and nano-alumina into CS, a more porous structure, as compared with the neat CS, was developed, thereby increasing the surface area and active sites on the surface of the nanocomposite. FESEM image of the nanocomposite after adsorption, as shown in Fig. 5d, proved the capture of MB by the adsorbent and the removal of that from the aqueous solution.

3.1.4. BET analysis

The nitrogen adsorption-desorption isotherms were employed to examine the pore size and pore volume of the nanocomposite. The surface area of the adsorbent was computed by the Brunauer-Emmett-teller method; also, the average pore size was assessed by the Barrett-Joyner-Halenda (BJH) model [32]. The obtained results are presented in Table 4. Based on Fig. 6, the isotherm of the nanocomposite could be matched with a type IV isotherm with a H_2 hysteresis loop, suggesting the mesoporous structure of CS/MCM-41/Nano-alumina, according to IUPAC classification. The BET studies also verified the results of FESEM imaging.

3.2. RSM approach for the optimization of MB adsorption on the nano adsorbent

Central composite design is the most well-known technique among different classes of RSM for the optimization of parameters [33], determination of the main variables and their interaction with the least number of experiments (Table 2). The polynomial regression is the most popular relation

Table 4
Characteristics calculated by BET method for the composite sample

Sample	Specific surface area $m^2 g^{-1}$	Pore volume $cm^3 g^{-1}$	Pore diameter nm
CS/MCM-41 (70%)/ nano-alumina (30%)	63.835	0.084	0.25
CS	4.0	0.1	3.5
MCM-41	986.0	–	–
Nano-alumina	76.0	–	–

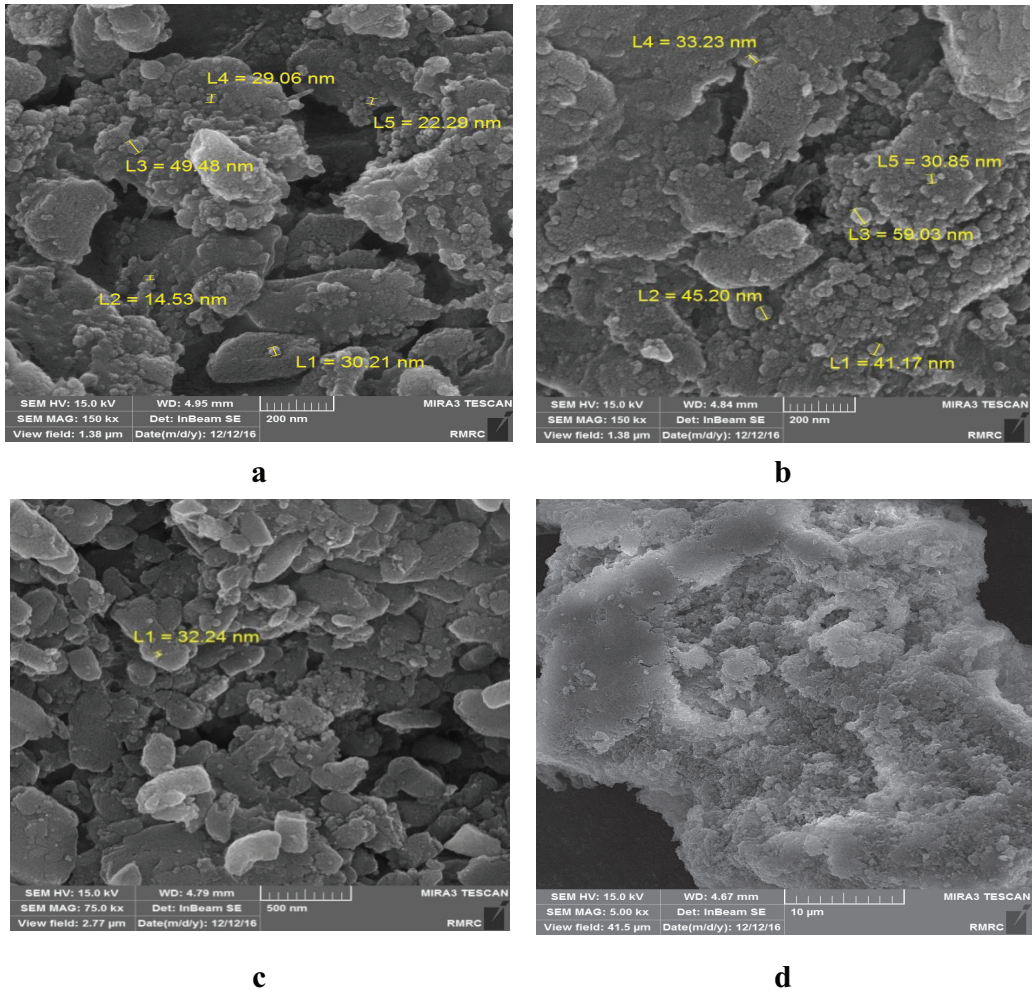

Fig. 5. FESEM images of a) CS/MCM-41 (30%)/nano-alumina (70%), b) CS/MCM-41 (50%)/nano-alumina (50%), c) CS/MCM-41 (70%)/nano-alumina (30%), and d) CS/MCM-41 (70%)/nano-alumina (30%) after adsorption of MB.

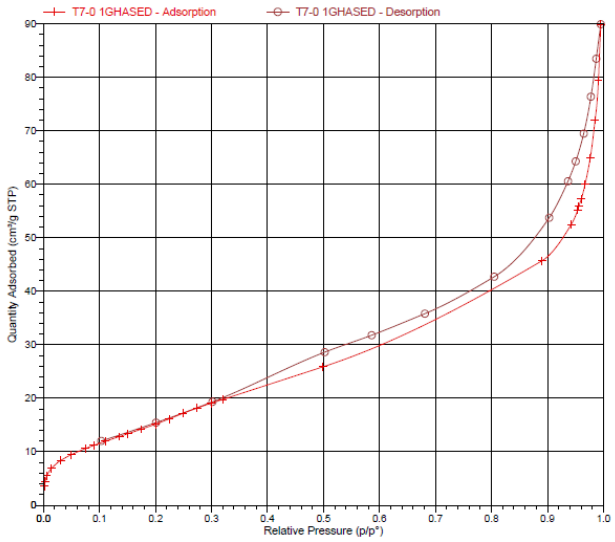

Fig. 6. N_2 adsorption-desorption isotherm of CS/MCM-41(70%)/nano-alumina (30%).

applied for the examination of the correlation between the variable and the response.

The results of the analysis of variance (ANOVA) and regression coefficients of MB revealed the high suitability of the quadratic model for the description of the adsorption behavior (significant with $p < 0.05$), as presented in Table 3. P-value related to the importance of each coefficient helped us to perceive the interactions among the variables. A p-value less than 0.05 in the ANOVA table represented the statistical significance of an effect at the 95% confidence level [34]. The "Lack of Fit (LOF) P-value" of 0.3246 showed that the LOF was not significant with regard to the pure error. The suitability of the polynomial model equation was stated by the coefficient of determination ($R^2 = 0.9911$ and adjusted $R^2 = 0.9814$) and represented the high degree of actual and predicted values. Regression analysis of CCD was done and the model equation was achieved:

$$\begin{aligned} Y = {} & -577.76050 + 79.45833x_1 - 1.48967x_2 + 43154x_3 + 9.00183x_4 \\ & +0.20167x_1x_2 - 3133.33x_1x_3 - 0.15x_1x_4 + 42.00x_2x_3 + 5.00000E \\ & -004x_2x_4 + 56.00x_3x_4 - 3.28x_1^2 - 0.0155x_2^2 - 1.44800E + 006x_3^2 \\ & -0.090500x_4^2 \end{aligned} \quad (4)$$

where Y (removal percentage) is the response referred to the predicted removal percentage of MB, and X_1, X_2, X_3 and X_4 are pH, the initial dye concentration, the adsorbent mass and the contact time, respectively. Figs. 7a–d present the response surface plots of removal (%) from CCD. The response surface plot is displayed by the pair of important factors at the fixed values of other factors. The curvatures of these plots proved the existence of the interaction between the variables. Each variable with a positive or negative coefficient showed its impact on the removal performance. The interactive impact of various parameters on the adsorption of the MB dye can be interpreted here:

The pH of a solution plays an important role in the adsorption of any adsorbate species because it monitors the surface charge of the adsorbent and degree of the ionization of the dye [35]. The influence of pH on MB adsorption was investigated in the range of 3–9; the results approved that the maximum removal percentage of the dye was acquired at pH 7.50. At this range, the electrostatic attraction between the positive charge of MB and the negative charge of the adsorbent was the main adsorption mechanism. As shown in Fig. 7a, removal efficiency was reduced at the low pH (<3), because of the saturation of the active sites of the adsorbent with hydrogen ions and the electrostatic repulsion between the dye and the surface of the adsorbent, while the increase in the removal efficiency with the rise in pH was due to less competition between protons and the dye for active sites and the enhancement of the negative surface charge, leading to more electrostatic attraction between the dye and the surface of the adsorbent. Therefore, the pH of the MB solution is a parameter controlling the adsorption of the dye.

The contact time between the adsorbent and adsorbate is one of the most prominent parameters in the adsorption process. The influence of the contact time on the removal efficiency was studied in the range of 35–55 min and the time of 45 min was considered as the optimum, as shown in Fig. 7b. It could be concluded that the adsorption capacity was enhanced with the growth of contact time, which could be attributed to the improved surface area and dispersion of the adsorbent into the solution.

The influence of the initial dye concentration on the adsorption capacity was examined in the range of 5–25 mg/L and the maximum removal efficiency was obtained at 15 ppm of the MB dye solution. The results are given in Fig. 7c. Based on the obtained results, at the lower concentration of MB, the removal percentage of the dye was improved owing to the low ratio of the solute concentration to the adsorbent sites, more vacant sites on the adsorbent, and more contact surface. In contrast, at the higher concentration of the dye, the removal efficiency was decreased due to the saturation of the surface of CS/MCM-41/nano-alumina. These results showed the high dependence of the adsorption performance on the initial MB concentration.

The effects of the adsorbent mass on the adsorption efficiency were studied by applying various amounts of the adsorbent, from 0.05 to 0.1 g. As presented in Fig. 7d, the adsorbed amount of MB by the adsorbent was sharply improved with the increase in the adsorbent mass. The increase in the number of unoccupied adsorption sites and the enhancement of surface area availability can be regarded as the reason. The adsorption amount became maximum when the adsorbent dose was increased to 0.008 g. Therefore, the amount of 0.008 g of the adsorbent mass was regarded as the optimum.

3.3. Adsorption equilibrium study

Adsorption equilibrium isotherm is expressed on the basis of the mathematical association of the amount of the adsorbed species per gram of the adsorbent (q_e *(mg/g)*) to the equilibrium non-adsorbed amount of the dye in solution (C_e *(mg/L)*) at the fixed temperature [36,37]. Adsorption equilibrium supplies the essential information to examine the suitability of the adsorption process. In the current study, Langmuir [38] and Freundlich [39] isotherm models were employed to investigate the adsorption mechanism. The results are presented in Table 5, and Langmuir

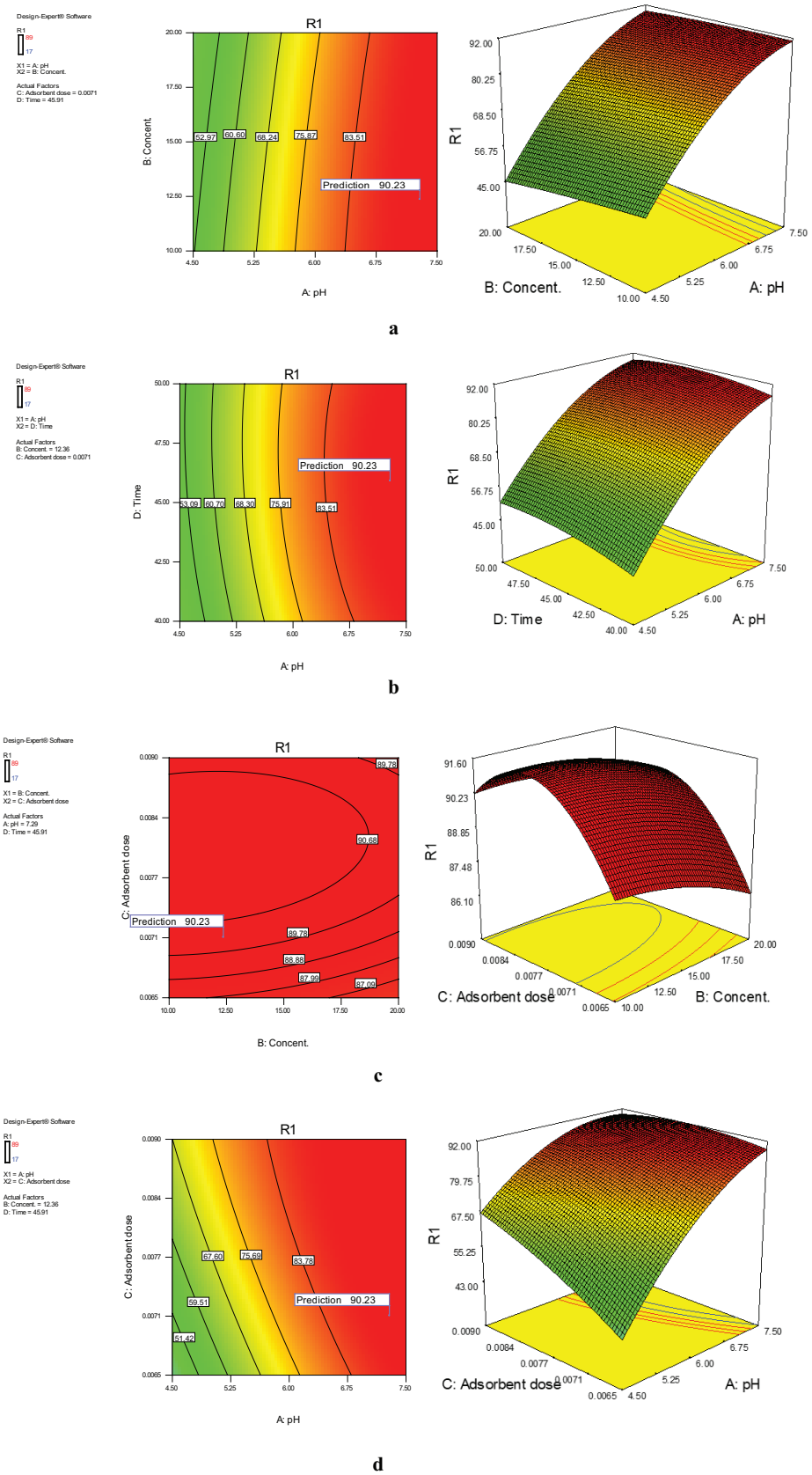

Fig. 7. The 3D response surface plots and contour plots for interactive influence of a) pH and initial dye concentration, b) pH and contact time, c) initial dye concentration and adsorbent dosage, and d) pH and adsorbent dosage.

Table 5
Isotherm constant parameters and correlation coefficients calculated for the removal of MB onto CS/MCM-41/nano-alumina composite.

Isotherm	Equation	Parameter	Value
Langmuir	$\frac{C_e}{q_e}=\frac{1}{K_l q_m}+\frac{C_e}{q_m}$	R^2	0.9955
		q_m	80.00 mg/g
		k_l	0.68 L/mg
Freundlich	$\ln q_e=\ln K_f+\frac{1}{n}\ln C_e$	R^2	0.9296
		n	1.92
		k_f	4.30 mg/g

q_m: maximum adsorption capacity (mg/g), k_l: Langmuir constant or adsorption equilibrium constant (L/mg), k_f: Freundlich constant concerned to capacity of adsorption, $1/n$: isotherm constant related to intensity of adsorption.

and Freundlich plots are shown in Fig. S1. The Langmuir adsorption constant (k_l) and theoretical maximum adsorption capacity (q_m) were calculated from the intercept and slope of the plot of C_e/q_e against C_e, respectively. The suitability of the Langmuir model for the explanation of the experimental data could be concluded from the high value of the correlation coefficient (R^2). The parameters of the Freundlich isotherm model, such as k_f and n (an indication of the capacity and intensity of the adsorption), were obtained from the intercept and slope of the linear plot of $ln\ q_e$ vs. $ln\ C_e$, respectively.

The linear fit between C_e/q_e vs. C_e and the computed correlation coefficient for the Langmuir isotherm model indicated its compatibility for fitting with the experimental data (Table 5) and proved that MB adsorption had occurred at specific homogeneous sites over the mono-layer pattern. The maximum adsorption capacity obtained from the Langmuir model was discovered to be 80 mg/g, which was comparable or even higher than those mentioned in Table 6. The greater ability of CS/MCM-41/nano-alumina for the MB adsorption could be ascribed to the large specific surface area and the negative functional groups in the MB adsorption process. A brief list of the adsorbents previously applied for MB adsorption study is presented in Table 6. It could be concluded that CS/MCM-41/nano-alumina possessed excellent adsorption capacity and could be applicable for new potential adsorption systems.

3.4. Adsorption kinetics

The purpose of the kinetic adsorption study was to describe the dynamics of the adsorption process in terms of the order of the rate constant. Hence, two kinetic models including the pseudo-first-order [51] and the pseudo-second-order [52] were examined to study the adsorption kinetic of the MB dye on the adsorbent. The properties and parameters of each kinetic model are presented in Table 7 and the plots of kinetic models are shown in Fig. S2. According to the experimental results, parameters such as k_1 (the rate constant of the pseudo-first-order adsorption (min^{-1})) and q_e (the adsorption capacity at equilibrium time (mg/g) were assessed from the slope and intercept of the plot of $log\ (q_e - q_t)$ versus t; also, the slope and intercept of the plot of t/q_t against t could give k_2 (the rate constant of the pseudo-second-order adsorption (g/mg/min)) and q_e (the adsorption capacity at equilibrium time (mg/g)). In addition, the value of the correlation coefficient (R^2) for the pseudo-second-order model was nearunity ($R^2 = 0.9856$) and higher than that of the pseudo-first-order model, thereby indicating the good fitness between the theoretical and experimental data and this model. On the other hand, the MB dye adsorption on the nanocomposite followed the pseudo-second-order kinetic model.

Table 6
Adsorption capacities of various adsorbents for removal of MB dye

Adsorbent	q_{max} (mg/g)	Reference
Activated carbon/urea-formaldehyde	1.4146	[40]
Silver nanoparticles loaded on activated carbon	71.4	[41]
Palladium nanoparticles loaded on activated carbon	75.4	[41]
Magnesium aluminate spinel	0.945	[42]
Tea waste/$CuFe_2O_4$	32.25	[43]
$LaFeO_3$	0.03	[44]
Hazelnut	76.9	[45]
Walnut	59.17	[45]
Cherry	39.84	[45]
Oak	29.94	[45]
Pitch-pine	27.78	[45]
Magnetic nay zeolite	2.046	[46]
Chitosan/activated clay	330.0	[47]
Cross-linked succinyl CS	289.0	[48]
CS- beads formed by sodium dodecyl sulfate	226.2	[48]
Cross linked chitosan/bentonite composite	142.9	[49]
NiO/MCM-41	24.50	[50]
CS/MCM-41/nano-alumina	80.00	Current study

3.5. Thermodynamic studies

The influence of the temperature variation on the adsorption process could be examined by thermodynamic studies [53]. Therefore, the temperature dependence of the adsorption process was investigated by employing various thermodynamic parameters such as Gibbs free energy change (ΔG°), standard enthalpy change (ΔH°) and standard entropy change (ΔS°), according to equations brought below:

$$\Delta G^\circ = -RTlnk_e \quad (5)$$

where k_e is thermodynamic equilibrium constant estimated from the equilibrium dye adsorption (q_e) and equilibrium dye concentration (C_e).

Table 7
Kinetic parameters for the removal of MB onto CS/MCM-41/nano-alumina composite

Model	Equation	Parameters	Value
Pseudo-first-order	$\log(q_e - q_t) = \log(q_e) - \frac{k_1 t}{2.303}$	k_1 (min^{-1}) q_e(calc)(mg g^{-1}) R^2	0.0944 99.58 0.9313
Pseudo-second-order	$\frac{t}{q_t} = \frac{1}{k_2 q_e^2} + \left(\frac{1}{q_e}\right)t$	k_2 (g mg^{-1} min^{-1}) q_e(calc)(mg g^{-1}) R^2	0.0007 59.52 0.9856

k_1: Rate constant of pseudo-first order adsorption (min^{-1}), k_2: second-order rate constant of adsorption(g mg^{-1} min^{-1}), q_e(calc): equilibrium capacity (mg g^{-1}).

$$K_e = q_e/C_e \quad (6)$$

Afterwards, the relation between ΔG°, ΔH° and ΔS° could be calculated by the following equation:

$$\Delta G° = \Delta H° - T\Delta S° \quad (7)$$

The value of ΔH° and ΔS° were assessed from the slope and intercept of the linear plot of lnk_e vs 1/T (Fig. S3, SI) in the following equation:

$$Lnk_e = \Delta S°/R - \Delta H°/RT \quad (8)$$

Also, ΔG° could be determined from the correct values of ΔH° and ΔS°. The results are presented in Table 8. Based on the obtained results in Table 8, the adsorption of MB on the CS/MCM-41/Nano-alumina was spontaneous and thermodynamically favorable because of the negative value of ΔG° at all tested temperatures. In addition, decreasing the negative values of ΔG° upon the increase in the temperature exibited that the adsorption process was less preferred at higher temperatures [54]. The endothermic nature of the adsorption process was proved by the positive value of ΔH°. The positive value of ΔS° suggested an increase in the randomness at the solid-liquid interface and freedom of the adsorbate during the adsorption process. Furthermore, the adsorption of MB on the nanocomposite was physisorption because ΔH° values were less than 40 kJ/mol and the ΔG° values were between –20 and 0 kJ/mol [55].

Table 8
The thermodynamic parameters for adsorption of MB onto synthesized nanocomposite

T (K)	lnK_e	ΔG° (kJ mol^{-1})	ΔH° (kJ mol^{-1})	ΔS° (kJ mol^{-1}K^{-1})	R^2
283.15	3.4549	–8.1332	7.2697	0.0537	0.9214
293.15	3.4648	–8.4445			
303.15	3.4634	–8.7291			
313.15	3.5972	–8.3653			
323.15	3.7995	–8.5081			
333.15	3.8875	–8.7675			

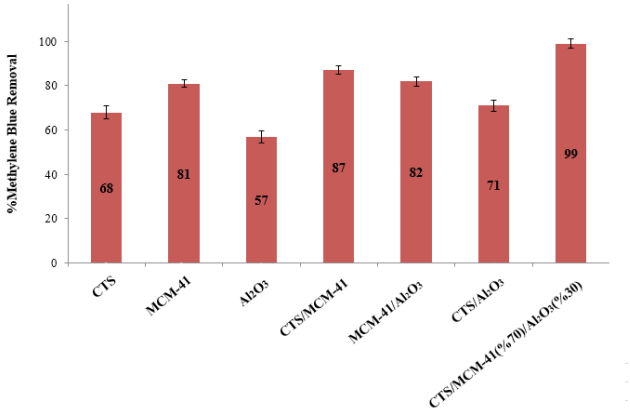

Fig. 8. The influence of different molar ratios of the nanocomposite and other adsorbents on the adsorption performance for removal of MB. Concentration: 10 mg/L; adsorbent dosage: 0.1 g; pH: 7; contact time: 30 min; temperature: 25°C.

3.6. Comparison of the adsorbents for elimination of MB dye

MB adsorption efficiency of the adsorbents with diverse molar ratios of the components are presented in Fig. 8. CS/MCM-41/Nano-alumina with 70 wt% MCM-41 and 30 wt% nano-alumina was considered as the optimum. It was clear that the removal efficiency of the optimum nanocomposite was much more than that of other adsorbents. In fact, synergistic effects produced by the combination of the components led to the intensified removal and the increased adsorption capacity of MB dye from the aqueous solution. Based on Fig. 11, the adsorption efficiency of the adsorbents for MB was in the order: CS/MCM-41 (70%)/nano-alumina (30%) > CS/MCM-41 > MCM-41/nano-alumina > MCM-41 > CS/nano-alumina > CS > nano-alumina.

3.7. TGA studies

Thermal degradation of the CS/MCM-41/nano-alumina composites in the different weight ratios were evaluated by TGA (Fig. 9). According to the results, with increasing the temperature the weight of three composites in the different weight ratios was decreased rapidly. The composites initial decomposition in the range of 55–100°C could be assigned to water evaporation. The weight loss of the organic component in the CS/MCM-41/nano-alumina composites occurred mostly in the range of 260–500°C.

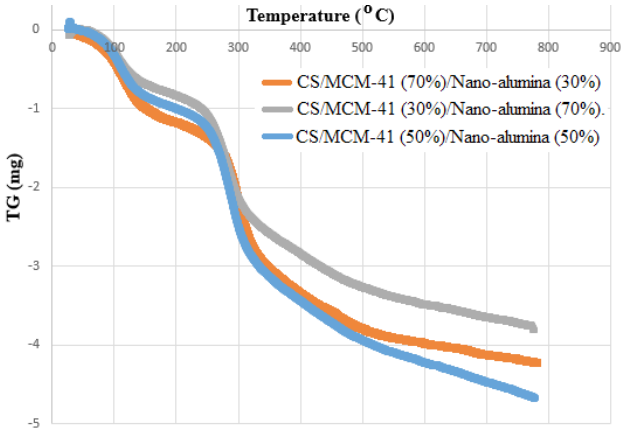

Fig. 9. TG curves of samples.

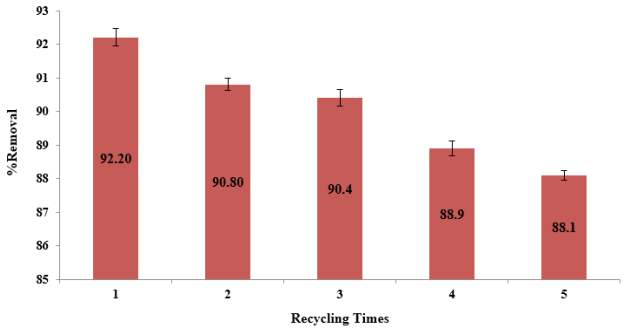

Fig. 10. Recyclability of CS/MCM-41(70%)/nano-γ alumina (30%) for MB adsorption in aqueous solution.

Since inorganic phase of CS/MCM-41(70%)/nano-alumina (30%), is less than CS/MCM-41(50%)/nano-alumina (50%) and CS/MCM-41(30%)/nano-alumina (70%).

3.8. Regeneration of the adsorbent

The main purpose of the desorption studies is to explain the nature of the adsorption process, regenarate the adsorbent, and recover the adsorbate. It has a close relationship with feasible usage in industries because the economy of the adsorption process relies on the regeneration of adsorbents [56]. In this paper, the recyclability of the adsorbent for the MB adsorption was examined in five cycles. As shown in Fig. 10, the removal efficiency of MB was reduced after five runs, indicating the reduction in the adsorption performance during the recycle process, which could be due to the incomplete desorption of the adsorbed sites of the adsorbent. However, the removal efficiency of MB remained above 88%, showing the excellent recyclability of CS/MCM-41(70%)/nano-γ alumina (30%) for practical applications. In addition, it should be mentioned that ethanol was selected as the optimum solvent for the desorption study.

3.8. Application to real sample

The usability of the developed method in this research was examined for the waste water of a loom factory containing the MB dye. Results are given in Table 9, indicating the good adsorption efficiency and consequently, the reliability of the proposed method for real samples.

Table 9
Calculation of removal efficiency in real sample

Concentration of MB in the sample before adding the adsorbed (ppm)	15
Concentration of MB in the sample after adding the adsorbent (ppm)	2.2
Removal efficiency	85.33

4. Conclusion

In the present study, CS/MCM-41/nano-γ alumina was synthesized and characterized by FTIR, XRD, FESEM, TGA and BET techniques. Then, it was used as a novel, efficient, and eco-friendly adsorbent for the removal of MB from the aqueous solution. The influence of parameters such as pH, contact time, adsorbent dosage, and the initial dye concentration was explored and optimized by CCD. The maximum removal efficiency under the optimum conditions (pH: 7.5, contact time: 45 min, adsorbent dosage: 0.088 mg, and initial dye concentration: 15 mg/L) was obtained to be 90.23%. The results revealed that the adsorption behavior could be described by the Langmuir isotherm with $R^2 = 0.9955$, and the maximum adsorption capacity of 80 mg/g, also kinetic data obeyed the pseudo-second-order model with $R^2 = 0.9856$. Thermodynamic studies also exhibited that the adsorption process was spontaneous and endothermic in nature. In addition, The MB adsorption efficiency after 5 adsorption-desorption cycles showed the high ability of the synthesized adsorbent for the MB sorption at the fifth cycle without any remarkable reduction in the sorption capacity, in comparison with the first cycle. The adsorption capacity of the adsorbents applied previously for the removal of MB was compared to the nanocomposite, confirming the high adsorption capacity of CS/MCM-41/nano-alumina in the elimination of MB. In addition, The present methodology might be helpful for designing the adsorbent useful in the treatment of actual effluents. The optimized method was employed to real samples. Finally, it should be mentioned that the synthesized nanocomposite is a technically applicable, very impressive, and environmental friendly adsorbent for the removal of MB, with a high potential for practical applications in water treatment industries.

Acknowledgements

We gratefully acknowledge the financial assistance provided by the Payame Noor University in Isfahan Research council(Grant No. 68424).

References

[1] A. Mohammadzadeh, M. Ramezani, A.M. Ghaedi, Synthesis and characterization of Fe_2O_3–ZnO–$ZnFe_2O_4$/carbon nanocomposite and its application to removal of bromophenol blue dye using ultrasonic assisted method: Optimization by response surface methodology and genetic algorithm, J. Taiwan Inst. Chem. Eng., 59 (2016) 275–284.

[2] D. Robati, B. Mirza, R. Ghazisaeidi, M. Rajabi, O. Moradi, I. Tyagi, et al, Adsorption behavior of methylene blue dye on nanocomposite multi-walled carbon nanotube functionalized thiol (MWCNT-SH) as new adsorbent, J. Mol. Liq., 216 (2016) 830–835.
[3] M. Roosta, M. Ghaedi, A. Daneshfar, R. Sahraei, A. Asghari, Optimization of the ultrasonic assisted removal of methylene blue by gold nanoparticles loaded on activated carbon using experimental design methodology, Ultrason. Sonochem., 21 (2014) 242–252.
[4] A. Asfaram, M. Ghaedi, S. Hajati, M. Rezaeinejad, A. Goudarzi, MK. Purkait, Rapid removal of Auramine-O and Methylene blue by ZnS: Cu nanoparticles loaded on activated carbon: a response surface methodology approach, J. Taiwan Inst. Chem. Eng., 53 (2015) 80–91.
[5] V. Sharma, P. Rekha, P. Mohanty, Nanoporous hyper-cross linked polyaniline: An efficient adsorbent for the adsorptive removal of cationic and anionic dyes, J. Mol. Liq., 222 (2016) 1091–1100.
[6] C. Li, J. Cui, F. Wang, W. Peng, Y. He, Adsorption removal of Congo red by epichlorohydrin-modified cross-linked chitosan adsorbent, Desal. Water. Treat., 57(30) (2016) 14060–14066.
[7] H. Karimi, M. Ghaedi, Application of artificial neural network and genetic algorithm to modeling and optimization of removal of methylene blue using activated carbon, J. Ind. Eng. Chem., 20 (2014) 2471–2476.
[8] A. Asfaram, M. Ghaedi, M.A. Azqhandi, A. Goudarzi, M. Dastkhoon, Statistical experimental design, least squares-support vector machine (LS-SVM) and artificial neural network (ANN) methods for modeling the facilitated adsorption of methylene blue dye, RSC Adv., 46 (2016) 40502–40516.
[9] A. Bhatnagar, E. Kumar, M. Sillanpää, Nitrate removal from water by nano-alumina: Characterization and sorption studies, Chem. Eng. J., 163 (2010) 317–323.
[10] ZA. Sutirman, M.M. Sanagi, K.J.A. Karim, W.A.W. Ibrahim, Preparation of methacrylamide-functionalized cross linked chitosan by free radical polymerization for the removal of lead ions, Carbohydr. Polym., 151 (2016) 1091–1099.
[11] J. Xie, C. Li, L. Chi, D. Wu, Chitosan modified zeolite as a versatile adsorbent for the removal of different pollutants from water, Fuel, 103 (2013) 480–485.
[12] Y. Haldorai, J.-J. Shim, An efficient removal of methyl orange dye from aqueous solution by adsorption onto chitosan/MgO composite: A novel reusable adsorbent, Appl. Surf. Sci., 292 (2014) 447–453.
[13] S. Sugashini, K.M.S. Begum, A. Ramalingam, Removal of Cr (VI) ions using Fe-loaded chitosan carbonized rice husk composite beads (Fe-CCRCB): Experiment and quantum chemical calculations, J. Mol. Liq., 208 (2015) 380–387.
[14] P. Hou, C. Shi, L. Wu, X. Hou, Chitosan/hydroxyapatite/Fe_3O_4 magnetic composite for metal-complex dye AY220 removal: recyclable metal-promoted Fenton-like degradation, Microchem. J., 128 (2016) 218–225.
[15] Q. Qin, J. Ma, K. Liu, Adsorption of anionic dyes on ammonium-functionalized MCM-41, J. Hazard. Mater., 162 (2009) 133–139.
[16] F.N. Azad, M. Ghaedi, A. Asfaram, A. Jamshidi, G. Hassani, A. Goudarzi, M.H.A. Azqhandi, A. Ghaedi, Optimization of the process parameters for the adsorption of ternary dyes by Ni doped FeO (OH)-NWs–AC using response surface methodology and an artificial neural network. RSC Adv., 6 (2016) 19768–19779.
[17] A. Teimouri, S.G. Nasab, N. Vahdatpoor, S. Habibollahi, H. Salavati, A.N. Chermahini, Chitosan /Zeolite Y/Nano ZrO_2 nanocomposite as an adsorbent for the removal of nitrate from the aqueous solution, Int. J. Biol. Macromol., 93 (2016) 254–266.
[18] A. Teimouri, S. Ghanavati Nasab, S. Habibollahi, M. Fazel-Najafabadi, A.N. Chermahini, Synthesis and characterization of a chitosan/montmorillonite/ZrO_2 nanocomposite and its application as an adsorbent for removal of fluoride, RSC Adv., 5 (2015) 6771–6781.
[19] S.G. Nasab, A. Semnani, A. Teimouri, H. Kahkesh, T.M. Isfahani, S. Habibollahi, Removal of Congo Red from aqueous solution by hydroxyapatite nanoparticles loaded on zein as an efficient and green adsorbent: response surface methodology and artificial neural network-genetic algorithm, J. Polym. Environ., (2018) 1–21.
[20] M. Vallet-Regi, A. Ramila, R. Del Real, J. Pérez-Pariente, A new property of MCM-41: drug delivery system, Chem. Mater., 13 (2001) 308–311.
[21] M. Grün, K.K. Unger, A. Matsumoto, K. Tsutsumi, Novel pathways for the preparation of mesoporous MCM-41 materials: control of porosity and morphology, Microporous Meso porous Mater., 27 (1999) 207–216.
[22] J. Zhang, Q. Zhou, L. Kinetic, Isotherm, and thermodynamic studies of the adsorption of methyl orange from aqueous solution by chitosan/alumina composite, J. Chem. Eng. Data., 57 (2012) 412–419.
[23] W.M. Golie, S. Upadhyayula, Continuous fixed-bed column study for the removal of nitrate from water using chitosan/alumina composite, J. Water Process Eng., 12 (2016) 58–65.
[24] Y. Guo, D. Liu, Y. Zhao, B. Gong, Y. Guo, W. Huang, Synthesis of chitosan-functionalized MCM-41-A and its performance in Pb (II) removal from synthetic water, J. Taiwan Inst. Chem. Eng., 71 (2017) 537–545.
[25] S. Hassani, M. Shirani, A. Semnani, M. Hassani, Removal of Congo red by magnetic nano-alumina using response surface methodology and artificial neural network, Desal. Water Treat., 62 (2017) 241–251.
[26] A.M. Ghaedi, M. Ghaedi, A.R. Pouranfard, A. Ansari, Z. Avazzadeh, A. Vafaei, I. Tyagi, S. Agarwal, V.K. Gupta, Adsorption of triamterene on multi-walled and single-walled carbon nanotubes: Artificial neural network modeling and genetic algorithm optimization, J. Mol. Liq., 216 (2016) 654–665.
[27] E.A. Dil, M. Ghaedi, A. Ghaedi, A. Asfaram, M. Jamshidi, M.K. Purkait, Application of artificial neural network and response surface methodology for the removal of crystal violet by zinc oxide nanorods loaded on activate carbon: kinetics and equilibrium study, J. Taiwan Inst. Chem. Eng., 59 (2016) 210–220.
[28] E.A. Dil, M. Ghaedi, A. Asfaram, A. Goudarzi, Synthesis and characterization of ZnO-nanorods loaded onto activated carbon and its application for efficient solid phase extraction and determination of BG from water samples by micro-volume spectrophotometry, New J. Chem., 39 (2015) 9407–9414.
[29] A. Asfaram, M. Ghaedi, S. Hajati, A. Goudarzi, A.A. Bazrafshan, Simultaneous ultrasound-assisted ternary adsorption of dyes onto copper-doped zinc sulfide nanoparticles loaded on activated carbon: optimization by response surface methodology, Spectrochim, Acta A Mol. Biomol. Spectrosc., 145 (2015) 203–212.
[30] A.M. Elbarbary, M.M. Ghobashy, Phosphorylation of chitosan/HEMA interpenetrating polymer network prepared by γ-radiation for metal ions removal from aqueous solutions, Carbohydr. Polym., 162 (2017) 16–27.
[31] A.C. Pradhan, K. Parida, Facile synthesis of mesoporous composite Fe/Al_2O_3–MCM-41: an efficient adsorbent/catalyst for swift removal of methylene blue and mixed dyes, J. Mater. Chem., 22 (2012) 7567–7579.
[32] A.A. El-Bindary, A.Z. El-Sonbati, A.A. Al-Sarawy, K.S. Mohamed, M.A. Farid, Removal of hazardous azopyrazole dye from an aqueous solution using rice straw as a waste adsorbent: Kinetic, equilibrium and thermodynamic studies. Spectrochim, Acta A Mol. Biomol. Spectrosc., 136 (2015) 1842–1849.
[33] A. Ahmad, B. Hameed, A. Ahmad, Removal of disperse dye from aqueous solution using waste-derived activated carbon: Optimization study, J. Hazard. Mater., 170 (2009) 612–619.
[34] A. Asfaram, M. Ghaedi, A. Goudarzi, M. Soylak, S.M. Langroodi, Magnetic nanoparticle based dispersive micro-solid-phase extraction for the determination of malachite green in water samples: optimized experimental design, New J. Chem., 39 (2015) 9813–9823.
[35] V. Srivastava, Y. Sharma, M. Sillanpää, Response surface methodological approach for the optimization of adsorption process

in the removal of Cr (VI) ions by $Cu_2(OH)_2CO_3$ nanoparticles, Appl. Surf. Sci., 326 (2015) 257–270.
[36] A. Asfaram, M. Ghaedi, S. Agarwal, I. Tyagi, V.K. Gupta, Removal of basic dye Auramine-O by ZnS: Cu nanoparticles loaded on activated carbon: optimization of parameters using response surface methodology with central composite design, RSC Adv., 5 (2015) 18438–18450.
[37] Y.-S. Ho, G. McKay, The kinetics of sorption of divalent metal ions onto sphagnum moss peat, Water Res., 34 (2000) 735–742.
[38] I. Langmuir, The adsorption of gases on plane surfaces of glass, mica and platinum, JACS. 40 (1918) 1361–1403.
[39] V. Vadivelan, K.V. Kumar, Equilibrium, kinetics, mechanism, and process design for the sorption of methylene blue onto rice husk, J. Colloid Interface Sci., 286 (2005) 90–100.
[40] A. Kareem, N.A. Alrazak, K.H. Aljebori, A.M. Aljeboree, H.L. Algboory, A.F. Alkaim, Removal of methylene blue dye from aqueous solutions by using activated carbon/urea-formaldehyde composite resin as an adsorbent, Int. J. Chem. Sci., 14 (2016) 21–27.
[41] M. Ghaedi, S. Heidarpour, S.N. Kokhdan, R. Sahraie, A. Daneshfar, B. Brazesh, Comparison of silver and palladium nanoparticles loaded on activated carbon for efficient removal of Methylene blue: Kinetic and isotherm study of removal process, Powder Technol., 228 (2012) 18–25.
[42] B. Ismail, S.T. Hussain, S. Akram, Adsorption of methylene blue onto spinel magnesium aluminate nanoparticles: adsorption isotherms, kinetic and thermodynamic studies, Chem. Eng. J., 219 (2013) 395–402.
[43] S. Hashemian, M.K. Ardakani, H. Salehifar, Kinetics and thermodynamics of adsorption methylene blue onto tea waste/$CuFe_2O_4$ composite. Am, J. Analyt. Chem., 4 (2013) 1–11.
[44] S. Hashemian, M. Monshizadeh, Removal of methylene blue from aqueous solution by nano $LaFeO_3$ particles. Main Group Chem., 12 (2013) 113–124.
[45] F. Ferrero, Dye removal by low cost adsorbents: Hazelnut shells in comparison with wood sawdust, J. Hazard. Mater., 142 (2007) 144–152.
[46] M. Shirani, A. Semnani, H. Haddadi, S. Habibollahi, Optimization of simultaneous removal of methylene blue, crystal violet, and fuchsine from aqueous solutions by magnetic nay zeolite composite, Water Air Soil Pollut., 225 (2014) 2054–2062.
[47] M.-Y. Chang, R.-S. Juang, Adsorption of tannic acid, humic acid, and dyes from water using the composite of chitosan and activated clay, J. Colloid Interface Sci., 278 (2004) 18–25.
[48] S. Saber-Samandari, S. Saber-Samandari, N. Nezafati, K. Yahya, Efficient removal of lead (II) ions and methylene blue from aqueous solution using chitosan/Fe-hydroxyapatite nanocomposite beads, J. Environ. Manage., 146 (2014) 481–490.
[49] Y. Bulut, H. Karaer, Adsorption of methylene blue from aqueous solution by cross linked chitosan/bentonite composite, J. Dispersion Sci. Technol., 36 (2015) 61–67.
[50] X. Xiao, F. Zhang, Z. Feng, S. Deng, Y. Wang, Adsorptive removal and kinetics of methylene blue from aqueous solution using NiO/MCM-41 composite, Physica. E. Low Dimens. Syst. Nanostruct., 65 (2015) 4–12.
[51] Y. Ho, J. Ng, G. McKay, G. McKay Kinetics of pollutant sorption by biosorbents. Separation and purification methods, 29 (2000) 189–232.
[52] Y.-S. Ho, G. McKay, Pseudo-second order model for sorption processes, Process Biochem., 34 (1999) 451–465.
[53] V. Kumar, Adsorption kinetics and isotherms for the removal of rhodamine B dye and Pb^{2+} ions from aqueous solutions by a hybrid ion-exchanger, Arab. J. Chem., 2016.
[54] M.Y. Nassar, T.Y. Mohamed, I.S. Ahmed, I. Samir, MgO nanostructure via a sol-gel combustion synthesis method using different fuels: an efficient nano-adsorbent for the removal of some anionic textile dyes, J. Mol. Liq., 225 (2017) 730–740.
[55] M.Y. Nassar, M.M. Moustafa, M.M. Taha, Hydrothermal tuning of the morphology and particle size of hydrozincite nanoparticles using different counterions to produce nanosized ZnO as an efficient adsorbent for textile dye removal, RSC Adv., 48 (2016) 42180–42195.
[56] Y. Liu, W. Chen, H.-I. Kim, Removal of lead and nickel ions from wastewater by genipin cross linked chitosan/poly (ethylene glycol) films, J. Macromol. Sci., 49 (2012) 242–250.

Supporting Information

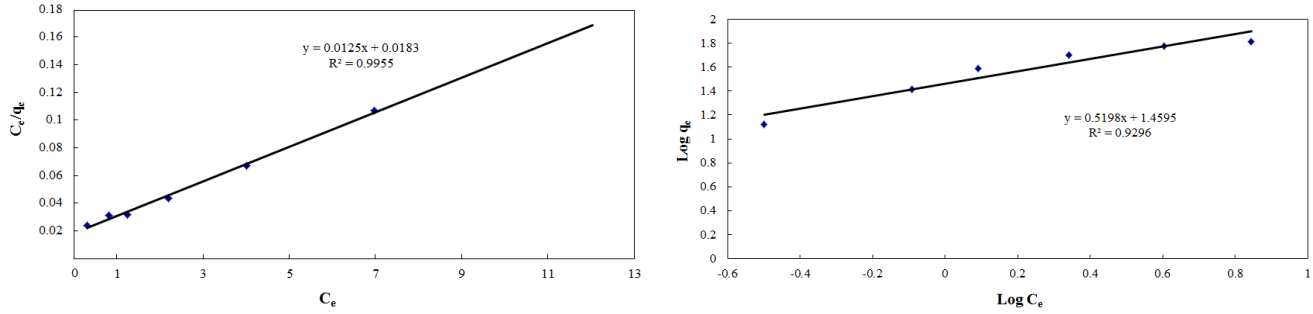

(a) (b)

Fig. S1. a) Langmuir adsorption isotherm and b) Freundlich adsorption isotherm for CS/MCM-41 (70%)/Nano-alumina (30%).

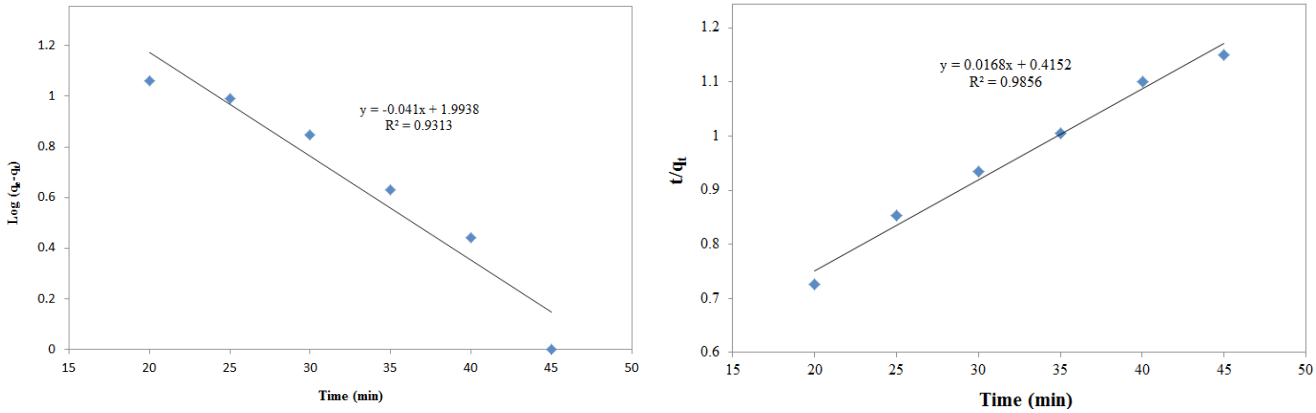

(a) (b)

Fig. S2. a) pseudo-first-order kinetic model and b) pseudo-second-order for MB adsorption by CS/MCM-41 (70%)/Nano-alumina (30%).

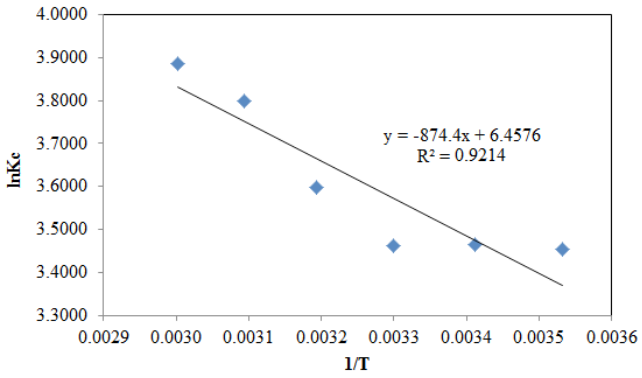

Fig. S3. Plot of ln k_e vs 1/T for MB adsorption onto CS/MCM-41 (70%)/Nano-alumina (30%).